ACS OMEGA

http://pubs.acs.org/journal/acsodf

Article

Conductivity of Multicomponent Alloy under Solid Solution Short-Range Order Cluster Model

Liang Huang,* Yan Cao, Shoumin Wang, Gaohong Li, Hao Dong, Tao Wu, and Ning Wang

Cite This: *ACS Omega* 2023, 8, 11987−11998

Read Online

ACCESS | Metrics & More | Article Recommendations

ABSTRACT: The characteristic of short-range order of multicomponent alloy solid solution promotes the necessity of deeply studying and establishing the microatomic structure behind the alloy components as well as the association with the corresponding macro-physical properties, so as to guide the development of high-performance multicomponent alloys through effective composition theory design. In this research, the popular Inconel 718 nickel-base superalloy with wide application and development is taken as an example. On the one hand, on the basis of the method of "the nearest neighbor cluster plus connecting atom" qualitatively proposed by predecessors to characterize the short-range order atomic arrangement structure of multicomponent alloy solid solution due to the interaction between electrons of atoms introduced into solid solution, Friedel oscillation potential function is generated and associated with the radial density of the corresponding atomic arrangement. On the other hand, according to the construction method of the nearest neighbor cluster in alloy phase that proposes the definition of using the maximum density of atomic radial arrangement to meet the minimum principle of energy stacking, the creatively accurate expression on the spatial structure of short-range order cluster of multicomponent alloy solid solution is achieved in a quantitative manner. Furthermore, with the impact of spatial distribution content of atoms in multicomponent alloy on the external current electron scattering rate (i.e., resistivity), the accurate analysis on the conductivity of multicomponent alloy by using the short-range order cluster model of alloy solid solution is realized through the weighting idea of atomic content of each element to the resistivity (the prediction rate is within 5%).

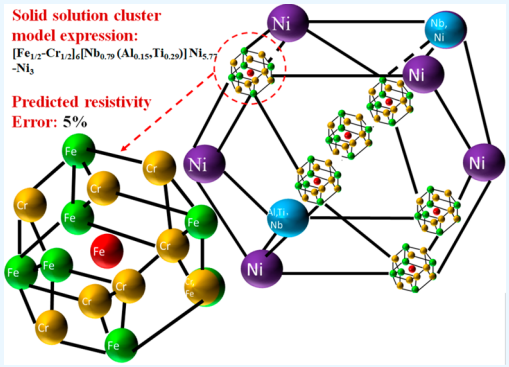

1. INTRODUCTION

In engineering practice, multicomponent alloys are usually formed by adding an appropriate element solid solution to metallic simple substances (i.e., alloying method) for improving the physical properties of metals and by virtue of whose material development mode characterized by broadness (i.e., different solid solution strengthening components introduced in the same matrix will show different physical properties by forming different phases) and specificity (i.e., it will show the optimal physical property at a specific alloy composition ratio), numerous solid-solution-structure-based industrial alloys in multicomponent system have been formed, with the emphasis on improvement of comprehensive mechanical strength and electrical conductivity.[1,2] For example, the excellent electrochemical characteristics unique to both Bi and Si make Al−Bi−Si alloy[3,4] widely used as an electrical contact switch material; featured by regular fibrous structure, Cu−Pb−Al, Cu−Pb−Zn and other alloys still maintain unique lubrication characteristics of Pb, thus becoming good bearing materials. A general lack of knowledge about the traceability of composition formation of industrial alloys has directly led to a long-term massive empirical exploration for the components of high-quality alloys and a great waste of energy and financial resources in the researches on new alloys. However, on the one hand, it was found from a large amount of practices and explorations in the early stage that the solid solution of an alloy shows a structure characterized by long-range disorder and short-range order,[5] so the investigations of the interatomic interaction mechanism from the perspective of short-range order spatial distribution structure of solid solution is the key to understand the origin of alloy phase composition. On the other hand, a large number of microscopic defects (movement dislocation, lattice deformation caused by the precipitation of the second phase, etc.) inside the crystals caused by alloying process will produce a fatal impact on its electrical conductivity when the strength of the alloy is enhanced.[6] Therefore, the establishment of an effective alloyed solid solution theory and a microscopic solid solvent analysis model and correlation with

Received: November 30, 2022
Accepted: February 24, 2023
Published: March 27, 2023

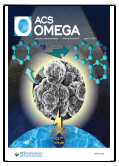

the macroscopic electric conductivity of alloys plays a decisive role in guiding the component design under multiple alloys. So, investigators at home and abroad have made the following detailed and in-depth researches on the microscopic solid solution model of multicomponent alloy and its mapping relation to macroscopic resistivity.

First, we will discuss the building of a microsolid solution model of multicomponent alloy. According to the indication of neutron diffraction and XRD analysis, the solid solution of multicomponent complex alloy is characterized by strong short-range order, whose heterogeneous atoms with negative enthalpy of mixing are prone to form the stable first neighbor coordination polyhedron, thus leading to the concept of cluster.[7] Based on the above, scholars proposed to use coordination polyhedron clusters as basic structural units to describe the structure of substances. For example, Bragg[8] used SiO_4 tetragonal polyhedron clusters as early as 1930 when defining silicide; then, DRPHS was put forward by Bernal[9] as a simple metal liquid model; at the same time, Chen and Dong[10] added that this model can be used to describe metallic glass; in 1973, Mackay et al.[11] further pointed out the feasibility of introducing a coordination polyhedron into the description on a complex solid solution to replace the atomic position and symmetry in traditional crystallography, but with the failure of forming normative description method based on the cluster structure. According to the principle that the greater the negative mixing enthalpy of mutual attraction between components, the greater the difference in atomic size, and the easier it is to form clusters, with the consideration of the specific alloy solid solution structure as the source for cluster configuration (that is, this local cluster structure representing the structural characteristics of alloy solid solution is related to the performance characteristics), an alloy solid solution with obvious cluster characteristics can be called cluster alloy solid solutions. Therefore, a group of colleagues at Dalian University of Technology[12−15] further proposed a universal any-structure-targeted cluster expression method, namely, [cluster] (connecting atom)x (that is, any solid solution structure can be expressed by the way of clustering plus connecting atom), but the accurate construction method of clusters has not been solved. From the crystallographic point of view, the cluster is composed of the nearest atom around a certain atom, but in fact, being often not on the same radius, the cluster shell needs to be divided into several layers, such as the Ni-centered layered structure Ni−Zr6−Zr3-Ni2 in Al2NiZr6 alloy phase. Meanwhile, the specific cluster construction method (that is, calculate the close packing degree of clusters contained in each shell to meet the principle of minimum energy stacking) was further put forward by relevant scholars in previous investigations through the use of Miracle close packing[16] and close packing rate,[17] which can accurately provide the specific definition of a cluster from the close packing point of view, but the consideration that the atomic radius is not a fixed value with the complexity in usage makes it necessary to put forward a simpler and more feasible construction method of the universal cluster model, so as to facilitate the construction and analysis of various alloy clusters. Then, there were additional investigations on the building of conductivity association mapping model. In order to characterize the resistivity of metal materials, the free-electron theory in metal conductors[18] was first put forward by Paul Drude, that is, when passing through metal lattice, free electrons collide with the positive ions in the metal lattice to scatter and obey the Maxwell−Boltzmann distribution under the action of electric field formed by positive ions in the metal lattice, thus generating the resistivity; the electron scattering motion described by this model is quite different from the reality, and then after the establishment of Fermi Dirac statistical theory, according to the combination with crystal band theory, it is believed that the potential field inside the idealized complete metal crystal has complete periodicity, which means that the scattering probability of external current electrons under the action of lattice potential field energy is 0 when making a transition under the action of electric field of external power supply, so the characteristic that the resistivity is 0 due to the obstruction of external current electrons does not exist in the metal material.[19] However, in the actual situation, the positive ions in the metal will deviate from the original lattice point due to thermal vibration at a certain temperature and trigger the deformation of the original lattice and the dissolving other elements in metal, which both cause the changes in the periodic potential field of the original crystal under ideal conditions, thus the occurrence of scattering during the passing of the above external current will form resistivity,[20] and then Ma Xisen, a famous British mathematician, put forward the empirical model of resistivity calculation (Matthiessen Rule) for low-concentration solid solution alloys; however, in recent years, the wide application and appearance of high-concentration solid solution alloys such as superalloys, high-entropy alloys, etc., as well as the large linear deviation between the resistivity predicted by Matthiessen Rule and the actual measured results in some low-concentration solid solution alloys, have all pushed scholars to further conduct researches on electronic spectrum of dilute solid solutions.[21−26] Thereby it is found that when other elements are added into alloy matrix element, they will show the short-range order of the solid solution after their rearrangement in the solid solution stage through the interactions between atoms, thus forming a short-range order model, while at the same time, the increasing contents of solid solution elements (from dilute solid solution to high solid solution) will make this short-range order structure gradually evolve into a long-range order structure or even a complete order structure in the whole solid solution structure. Based on this, an important thought to use chemical short-range order structure of solid solution for the characterization of alloy resistivity[27−30] was first proposed by Professor Tian Shan (1985) of the University of Aeronautics and Astronautics, thus associating the microscopic cluster model of alloy solid solution with the macroscopic resistivity. At the same time, a large number of experimental studies also show that,[31,32] the resistivity of alloy is mainly composed of the superposition of two-part scattering rate (as shown in formula (1), that is, the first part is the inherent resistivity formed by electron scattering that is caused by thermal vibration of the matrix lattice, while the other part is the additional resistivity formed by extra electron scattering that is caused by lattice deformation when other elements are dissolved in the matrix). Then, based on Mackay's method of using nearest neighbor coordination cluster to describe the complex solid solution structure,[33,34] as well as the analysis on the changes in resistivity when 1 atom % (atomic content) solid solution element is dissolved into the matrix, the Dong Chuang team of Dalian University of Technology[35] built a quantitative expression model of the overall resistivity of solid solution alloys through the way of using matrix resistivity as the inherent resistivity and using the resistivity when nat% solid solution elements are dissolved into the matrix as the

https://doi.org/10.1021/acsomega.2c07644
ACS Omega 2023, 8, 11987−11998

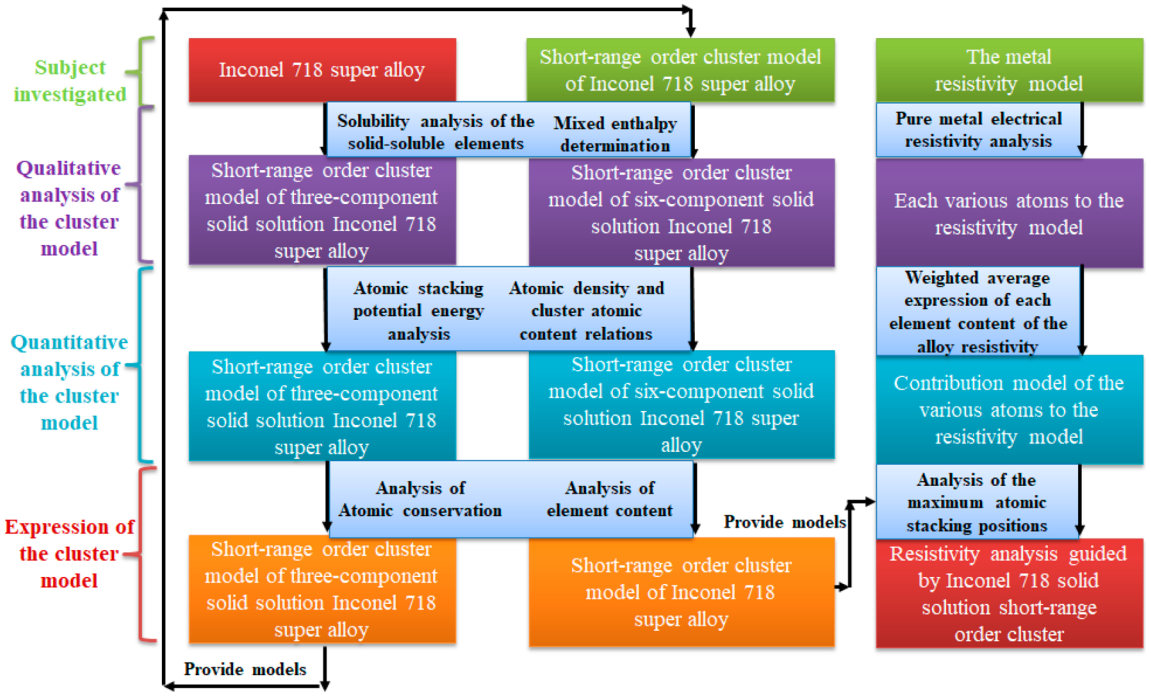

Figure 1. Research process of this paper.

additional resistivity (n represents the atomic content of solid solution element in solid solution matrix), with the achievement of accurate prediction on Cu−Ni−Si, metallic glass and other materials as well as the development of corresponding solid-solution alloys featured by high resistivity and high conductivity. However, the cluster resistivity characterization model is based on a large number of comparative experimental measurements and linear fitting analysis to obtain the change in the overall resistivity of alloys caused by the 1 atom % atomic solid solution/precipitation, but without further considering that the generation mechanism of the above-mentioned two-part resistivity of alloy is both that the final formation of scattering resistivity is due to the Coulomb collision of electron with the atoms inside the material crystal under the change of atomic potential field in material crystal (that is, the resistivity of alloy is unified with the species and spatial distribution mode of atoms in its crystal lattice). Therefore, a universal method for alloy resistance prediction under the guidance of cluster model needs to be put forward urgently.

$$\rho_{total} = \rho_{pho} + \rho_{imp} \quad (1)$$

Where ρ_{total} represents total resistivity of alloy; ρ_{pho} represents inherent resistivity of alloy matrix; ρ_{imp} represents additional resistivity caused by the dissolution of other elements into the alloy.

In this research, the popular Inconel 718 nickel-base superalloy composed of multiple elements with wide application and development is taken as the research object. Based on the method of "the nearest neighbor cluster plus connecting atom" qualitatively proposed by predecessors to characterize the short-range order atomic arrangement structure of multicomponent alloy solid solution, first, the short-range order cluster model of three-component Ni−Cr−Fe solid solution after adding a large amount of solid solution elements is qualitatively built according to the formation mechanism of Inconel 718 multielement alloy, with the combination of solid solution solubility and atomic mixing enthalpy criterion; at the same time, the short-range order cluster model of three-component Ni−Cr−Fe solid solution is quantitatively expressed through the way of introducing Friedel oscillation potential function generated by the interaction between electrons in solid solution atoms and the association with the radial density of corresponding atomic arrangement; second, based on the above model, the short-range order cluster model of six-component Inconel 718 alloy solid solution after adding trace strengthening elements is qualitatively built by further combining the solid solution solubility and atomic mixing enthalpy criterion, and according to the construction method of nearest neighbor cluster in alloy phase that proposing the definition of using the maximum density of atomic radial arrangement to meet the minimum principle of energy stacking, the corresponding atomic content of short-range order cluster model of Inconel 718 alloy solid solution formed by adding trace elements is determined, with the accuracy and rationality of the above-mentioned cluster model judged by combining element mass conservation, atomic conservation and atomic space stacking atoms, thus achieving the creatively accurate expression on the spatial structure of short-range order cluster of multicomponent alloy solid solution in a quantitative manner; finally, with the impact of spatial distribution content of atoms in multicomponent alloy on the external current electron scattering rate (i.e., resistivity), the accurate analysis on the conductivity of multicomponent alloy by using the short-range order cluster model of alloy solid solution is realized through the weighting idea of atomic content of each element to the resistivity (the prediction rate is within 5%, with the corresponding research process shown in Figure 1), thereby eventually achieving the accurate guidance for the conductivity of multicomponent superalloy and high-entropy alloy materials under the short-range order cluster model, which also lays the theoretical

https://doi.org/10.1021/acsomega.2c07644
ACS Omega 2023, 8, 11987−11998

foundation and research guarantee for the subsequent design and development of superalloy composition with high physical properties.

2. SHORT-RANGE CLUSTER ORDER MODEL BUILDING OF MULTICOMPONENT ALLOY SOLID SOLUTION

Due to the high content of solute of Inconel 718 nickel-base superalloy (as shown in Figure 2, non-Ni elements), the idea of short-range order cluster of solid solution is beneficial to realize the accurate prediction and expression on its resistivity. Meanwhile, the formation of Inconel 718 nickel-base superalloy is mainly by taking Ni element as the base for dissolution with the addition of many solid solution elements dominated by Fe and Cr during dissolution, followed by the addition of Nb, Al, and Ti-dominated trace strengthening elements to solid solution for precipitation strengthening through aging.[36] Considering that the atomic radius of Ni, Cr and Fe are similar (R_{Ni}: 0.124 nm, R_{Cr}: 0.127 nm and R_{Fe}: 0.127 nm), it is found by combining the solubility criterion of solid solution[37,38] that the elements Cr and Fe take the lead in forming unlimited solid solution with substitution characteristic in Ni base, and the impact of elastic strain caused by different atomic sizes on the atomic distribution in the solid solution alloy can be neglected, so the nearest-neighbor distribution between atoms in Ni−Cr−Fe solid solution alloy is mainly determined by the chemical action between elements (i.e., the enthalpy of mixing). Therefore, this paper puts forward first taking the element Ni matrix as basis to study the method of building short-range order cluster model of three-component solid solution with the introduction of massive solid-solution elements (Fe and Cr), and then based on the above model, studying the short-range order cluster model of six-component solid solution after introducing the trace strengthening

Composition of main elements of Inconel 718 alloy (this paper) (wt%)

Element	Content	Element	Content
Al	0.4200	Fe	18.0000
Cr	17.0000	Nb	5.3000
Ti	1.1000	Ni	55.0000

Figure 2. Distribution of components of Inconel 718 nickel-base superalloy.

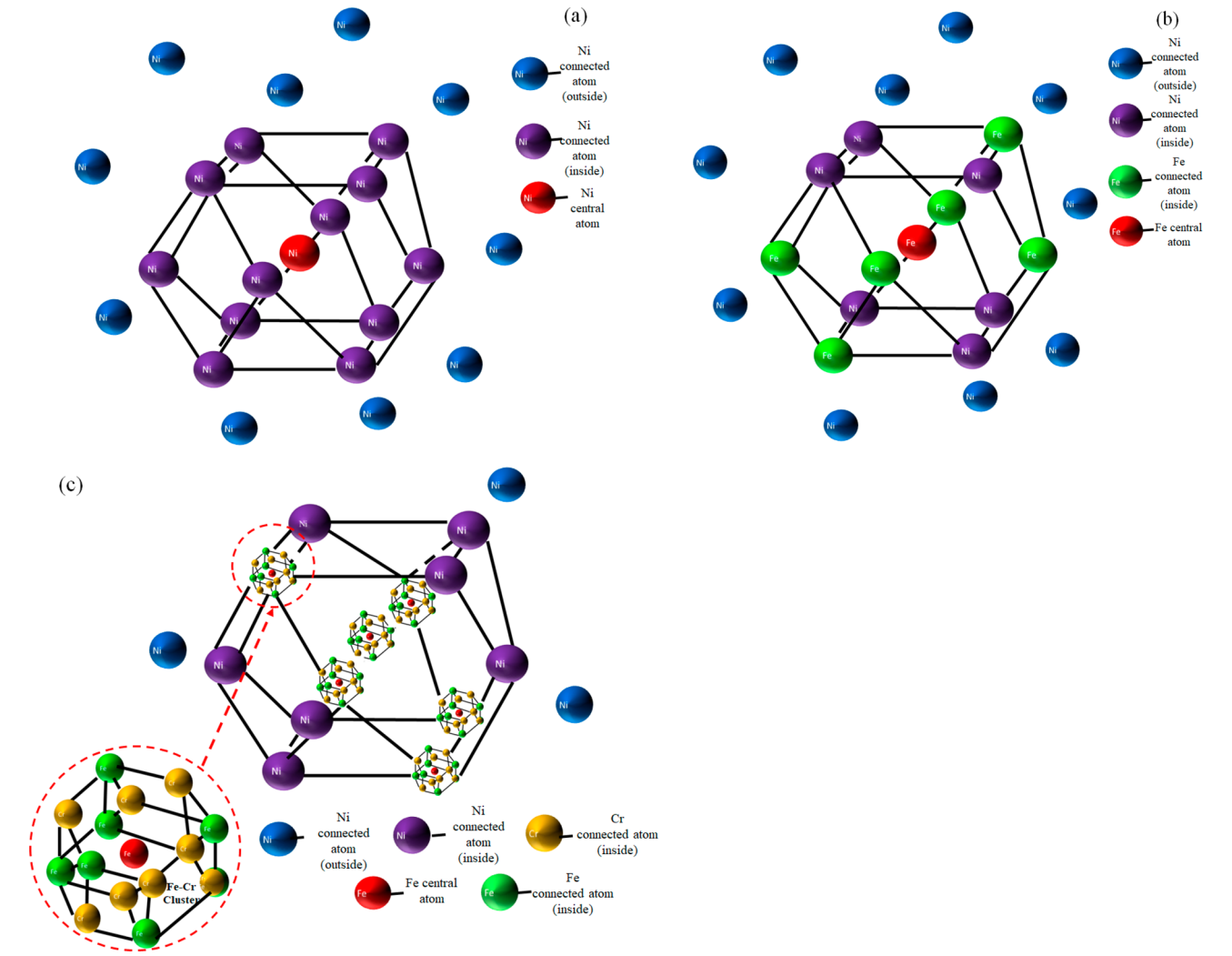

Figure 3. Short-range order cluster model of pure Ni matrix in (a), the short-range order cluster model of Ni−Fe solid solution in (b) and the short-range order cluster model of Ni−Fe−Cr solid solution in (c).

https://doi.org/10.1021/acsomega.2c07644
ACS Omega 2023, 8, 11987−11998

elements (Nb, Al and Ti), so as to accurately characterize the solid solution state of Inconel 718 nickel-base superalloy.

2.1. Short-Range Order Cluster Model Expression of Three-Component Ni−Cr−Fe Solid Solution. *2.1.1. Qualitative Expression on Short-Range Order Cluster Model of Three-Component Ni−Cr−Fe Solid Solution.* In the three-component solid solution of Ni−Cr−Fe, the matrix pure Ni is a cubic octahedron with a face-centered cubic structure (FCC), whose atomic spatial distribution structure can be expressed as $[Ni{-}Ni_{12}]$-Ni_y (as shown in Figure 3a, where $[Ni{-}Ni_{12}]$ refer to the centered part plus nearest neighbor coordination, while Ni_y refers to the connecting atom outside cluster). At the time of adding solid-solution elements Fe and Cr, $\Delta H_{Fe-Ni} = -2$ kJ/mol is the negative enthalpy of mixing (due to attraction, solute atoms tend to first occupy the central atom in solvent cluster), while$\Delta H_{Cr-Ni} = 12$ kJ/mol is the positive enthalpy of mixing (due to repulsion, solute atoms tend to occupy the connecting atoms outside solvent cluster),[39] so Fe atoms with higher content will successively replace the central atom and its adjacent connecting atoms in the Ni matrix cluster, thus forming the spatial distribution structure of $[Fe{-}Fe_xNi_{12-x}]$-Ni_y (as shown in Figure 3b); in addition, with Cr and Fe having the consistent atomic radius and crystal structure, $\Delta H_{Fe-Cr} = -1$ kJ/mol is the negative enthalpy of mixing, whileΔH_{Cr-Ni} is the positive enthalpy of mixing, and then considering the unlimited dissolution among Ni, Fe and Cr, on the premise of meeting the minimum principle of atomic stacking energy, Cr atoms will replace partial connecting atoms inside the above-mentioned cluster to locally form the cluster structure $[Fe_{x/15}$-$Cr_{15-x/15}]_yNi_{13-y}$ (as shown in Figure 3c, where $[Fe_{x/15}$-$Cr_{15-x/15}]$ represents that the structure of Fe−Cr solid solution is reduced to be treated as an atom).

2.1.2. Quantitative Expression on Short-Range Order Cluster Model of Three-Component Ni−Cr−Fe Solid Solution. The impact of electronic factors cannot be ignored during the consideration on the interaction between the specific numbers of atoms in the alloy, which is due to the dissolution of other atoms, and the introduction of a large number of extraneous electrons in the inherent atomic arrangement of base metal will trigger the interaction between the original electrons and the extraneous electrons, thus leading to the inevitable fluctuation of electron density of the system on the atomic microscopic scale. Therefore, in this paper, with the positive ions in the matrix metal lattice approximately regarded as the uniformly smoothed and continuously distributed positive-charge background, the shared electrons move on this positive background when the external power supply is connected, with the system maintaining the electroneutralization (i.e., the gel model) at the macro scale, while after dissolving the atoms of other elements, the generated extraneous electrons conducting interference on the electronic environment in the original matrix metal system will be shielded by the electrons inside its system through the way of rearrangement. Then, for any extraneous electron located at r, its realizably caused change in the total potential energy of electrons inside the metal system is proportional to a cosine function (i.e., Friedel oscillation,[40] as shown in formula (2)), while the reverse impact of this kind of electron−electron interaction on the interaction between atoms of a greater level (as shown in Figure 4) is reflected in the appearance of the maximum value in atomic stacking density (that is, the atomic density distribution function is the peak). The corresponding Friedel oscillation potential function shows a minimum value (that is, the Friedel oscillation potential function is the trough) due to the higher external electron density, but with the appearance of minimum value in atomic stacking density, the results of atomic density distribution function and Friedel oscillation potential function are opposite to the above; thereby, the radial distribution function of total atomic number density of alloy cluster model under different shells (as shown in formula (3)) can be introduced and associated with the above-mentioned corresponding Friedel oscillation potential function, so as to realize the control on the accuracy and rationality of the building of alloy cluster model.[41−44]

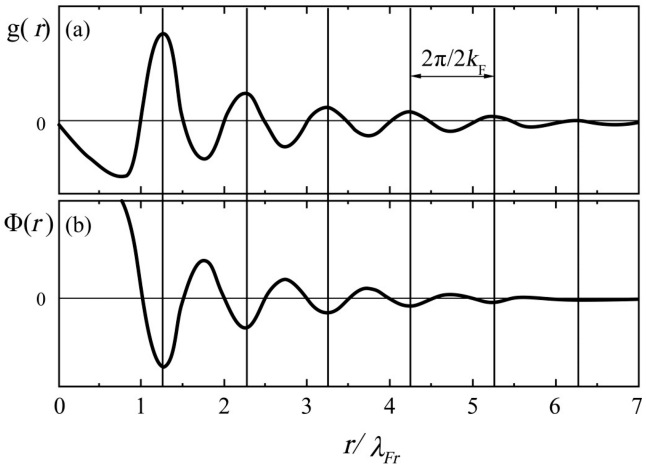

Figure 4. Atomic density distribution function in (a), and the corresponding electronic Friedel oscillation potential function ($\phi(r)\infty -\sin(2k_F{\cdot}r)/r^3$) in (b) (with the abscissa changed into r/λ_{Fr}).

$$\phi(r) \propto \cos(2k_F{\cdot}r + \Theta)/r^3 \tag{2}$$

$$g(r) = N(r)/(4\pi r^3/3) \tag{3}$$

where $g(r)$ represents total atomic distribution density (each shell); r represents distance from the central atom of cluster to the shell atom; $N(r)$ represents total number of atoms contained in the cluster with radius r; k_F represents Fermi wave vector; Θ represents phase shift. Many investigations show[45,46] that the phase shift Θ between amorphous liquid and metallic glass at short-range and medium-range distances is close to $\pi/2$, so its Friedel oscillation potential function can be characterized as $\phi(r)\infty -\sin(2k_F{\cdot}r)/r^3$), and it is defined that $\lambda_{Fr} = 2\pi/2k_F$.

Therefore, for the amorphous liquid and metallic glass, the combination of Figure 4 and formula 3 shows that the distribution interval of the first adjacent shell is $[\lambda_{Fr}, 1.5\ \lambda_{Fr}]$, with the distribution interval of the corresponding connecting atom as $[1.5\lambda_{Fr}, 2\lambda_{Fr}]$, and the distribution interval of the second adjacent shell is $[2\lambda_{Fr}, 2.5\lambda_{Fr}]$, with the distribution interval of the corresponding connecting atom as $[2.5\lambda_{Fr}, 3\lambda_{Fr}]$.... At the same time, for the guarantee of overall stability system through the minimum principle of atomic stacking energy, the peak with the highest density of stacking is more inclined to the location at $(n+1/4)\lambda_{Fr}$, n = 1,2,3....; however, the trough with the lowest density of stacking is more inclined to the location at $(n+3/4)\lambda_{Fr}$, n = 1,2,3....(that is, ball periodicity).

https://doi.org/10.1021/acsomega.2c07644
ACS Omega 2023, 8, 11987−11998

Considering the decisive role of the above Fermi wave vector k_F in the stability of amorphous liquid and metallic glass structure, as well as its relevance shown in formula (4) with the average atomic density ρ_a and the electron concentration e/a, the electron concentration is associated with the atomic content of cluster by Professor Luo of Dalian University of Technology, thus proposing the quantitative mapping relationship between the average atomic density ρ_a under a specific shell in the amorphous cluster and the number of its contained atoms Z when the Friedel oscillation occurs,[47] thereby the mapping relationship between the number of specific atoms contained in a single shell and its average atomic density when Friedel oscillation occurs can be deduced (as shown in formula (5)). In recent years, scholars' discovery and conformation on the existence of structural homology between amorphous liquid and its corresponding primary solid solution within the scope of short-range to medium range[48−50] makes it feasible to use this constraint condition to conduct calculation and analysis on the atomic weight of the above Ni−Cr−Fe solid solution cluster.

$$k_F = (3\pi^2 \cdot \rho_a \cdot e/a)^{1/3} \tag{4}$$

$$Z = c \cdot \rho_a \cdot r_1^3 \tag{5}$$

where c takes a constant of 11.476 (substitutional-type solid solution with high solute content)

Therefore, for the above-mentioned Ni−Cr−Fe solid solution cluster model $[Fe_{x/15}\text{-}Cr_{15-x/15}]_yNi_{13\text{-}y}$ of Inconel 718 nickel-base superalloy, based on the combination with its above-mentioned formation method, it can be divided and respectively expressed as a concentrated solid solution system $[A_x\text{-}Ni_{13-x}]\text{-}A_yNi_z$ with FCC structure (density ratio of 0.74) and a concentrated solid solution system $[Fe_x\text{-}Cr_{15-x}]$-A with BCC structure (density ratio of 0.68), so that the relationship shown in formula (6) is established by combining atomic conservation:

$$\begin{cases} 13+y+z = c\cdot(R_A+R_{Ni})^3/[\frac{x+y}{13+y+z}\cdot(4/3\pi\cdot R_A^3/0.74)+\frac{13-x+z}{13+y+z}\cdot(4/3\pi\cdot R_{Ni}^3/0.74)](\text{FCC}) \\ 1 = c\cdot(R_{Fe}+R_{Cr})^3/[\frac{x}{15}\cdot(4/3\pi\cdot R_{Fe}^3/0.68)+\frac{15-x}{15}\cdot(4/3\pi\cdot R_{Cr}^3/0.68)](\text{BCC}) \end{cases} \tag{6}$$

It is found from the respective solutions to the above formula that there are many possible combinations of x, y and z, but due to the required consistency between the atomic content (at%) of the built cluster model and the element mass content (wt %) of Inconel 718 nickel-base superalloy selected in Figure 2, the Ni−Fe−Cr solid solution cluster of Inconel 718 nickel-base superalloy corresponding to the optimal solution of formula (6) is finally determined as $[Fe_{1/2}\text{-}Cr_{1/2}]_6Ni_7{-}Ni_3$. In addition, the comparison between the element mass content in Ni−Fe−Cr solid solution cluster $[Fe_{1/2}\text{-}Cr_{1/2}]_6Ni_7{-}Ni_3$ and that in Inconel 718 nickel-base superalloy also shows that the content of Cr and Fe is similar to that of the selected grade, while the content of Ni is as high as 64.4, which is mainly because only the clusters corresponding to the composition of Ni−Fe−Cr three-component system alloy are considered above, without the introduction of trace elements. When being introduced, the trace elements Nb, Al and Ti will make the content of element Ni in the clusters further reduced by further replacing the Ni atoms in the above clusters, thus finally forming an accurate six-component cluster model consistent with grade content, and then the above-mentioned method will be used to study the solid solution cluster model building of Inconel 718 nickel-base superalloy after the introduction of trace elements.

2.2. Expression of Six-Component Inconel 718 Alloy Solid Solution by Short-Range Order Cluster Model. *2.2.1. Construction of a Short-Range Order Cluster Model for Six-Component Inconel 718 Alloy Solid Solution.* When the trace elements Nb, Al and Ti (R_{Nb}: 0.148 nm, R_{Al}: 0.143 nm and R_{Ti}: 0.145 nm) are continuously added on the basis of the three-component Ni−Cr−Fe solid solution obtained above, since the atomic radius of Al, Ti and Nb differs greatly from the radius of the first shell atom $[Fe_{1/2}\text{-}Cr_{1/2}]_6$ in the Ni−Fe−Cr cluster, the elements Nb, Al and Ti are hardly soluble in the first shell atom of the cluster. Considering that the atomic radii of Al, Ti and Nb are similar to that of Ni_7 atoms in the second shell (atomic radius difference Al−Ni: 15.3%; Ti−Ni: 16.9%, Nb−Ni: 19.3%; at the same time, a large number of practices prove that interstitial solid solutions are easy to form only when the ratio of solute atomic radius to solvent atomic radius is less than 0.59) and the outermost atom in the first shell layer has strong negative mixing enthalpy with Al, Ti and Nb elements, based on the principle of minimum energy, the addition of trace elements Al, Ti and Nb will form a solid solution cluster with lattice distribution through displacement with the Ni_7 atoms in the second shell of Ni−Fe−Cr solid solution cluster $[Fe_{1/2}\text{-}Cr_{1/2}]_6Ni_7{-}Ni_3$.

In addition, to further determine the number of atoms specifically displaced in the second shell Ni_7 after the introduction of the aforementioned trace elements, **a method of defining the nearest neighbor cluster in the alloy phase by the maximum atomic density was proposed herein.** The method comprises the following steps of: first, initiating all possible spatial atom distribution structures of corresponding precipitated phases according to the addition of trace elements; second, calculating and selecting a shell layer with the highest radial atom density and the most complete structure as the cluster structure most likely to be formed by the precipitated phases (i.e., meeting the atomic close packing principle) and thus reversely deducing the trace atom content of the final Inconel 718 alloy solid solution formed after the introduction of the trace elements according to the content proportion relation of each component. Therefore, the atomic arrangement information on each phase in Pearson Crystal Database was used and correlated with the phase distribution content of Inconel 718 nickel-base superalloy selected in this paper in the XRD phase analysis (as shown in Figure 5, since different molding methods can induce the differences of phase distribution and thus have influence on the construction of cluster model, the molded alloy under SLM+HSA aging treatment was selected as the phase distribution object). In addition, based on the core idea proposed by Formula (5) that the arrangement of cluster atoms is characterized by the distribution of each atom when the radial atomic density distribution function reaches the maximum value, and the analysis results shown in Tables 1 and 2, a solid solution cluster model corresponding to the γ'' phase and γ' phase formed by introducing trace elements (Al, Ti, and Nb) was established as $[Ni{-}Ni_8Nb_4]\text{-}Ni_3$ and $[Ni{-}Ni_8(Al,Ti)_4]\text{-}Ni_3$ (the mixing enthalpy relationship between the core atom and the outer layer atom was further considered when the atomic density was the same). Finally, by converting the solid solution cluster model corresponding to the γ'' phase and γ' into an atomic content proportional form ($[Ni_{9/16}Nb_{1/4}]\text{-}Ni_{3/16}$ and $[Ni_{9/16}(Al,Ti)_{1/4}]\text{-}Ni_{3/16}$) and combining with atom conserva-

https://doi.org/10.1021/acsomega.2c07644
ACS Omega 2023, 8, 11987−11998

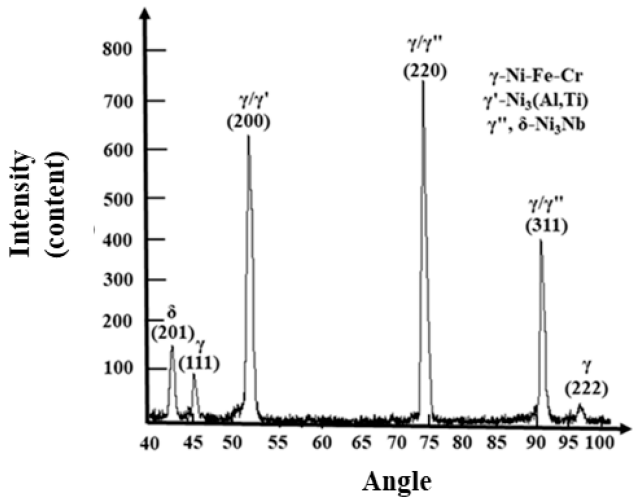

Figure 5. Phase analysis results of Inconel 718 alloy.

Table 1. Possible Different Atomic Occupation and Radial a Tomic Distribution Results of γ'' Phase

Core atoms	Number of outer layer atoms	Atomic species	Distance between the shell atom and the core atom (nm)	Atomic density (nm^{-3})
Ni	Ni	4	0.2514	135.34
	Nb	4	0.2570	183.10
	Ni	4	0.2570	239.44
Nb	Ni	4	0.2514	135.34
	Ni	8	0.2570	183.10

Table 2. Possible Different Atomic Occupation and Radial Atomic Distribution Results of γ' Phase

Core atoms	Number of outer layer atoms	Atomic species	Distance between the shell atom and the core atom (nm)	Atomic density (nm^{-3})
Ni	Ni	8	0.2539	131.39
	(Al, Ti)	4	0.2539	189.78
(Al, Ti)	Ni	12	0.2539	135.78

tion, the solid solution cluster model of Inconel 718 alloy after the introduction of trace strengthening elements was $[Fe_{1/2}\text{-}Cr_{1/2}]_6$ $[Nb_{0.79}$ $(Al_{0.15},Ti_{0.29})]Ni_{5.77}\text{-}Ni_3$ by Formula (6).

2.2.2. Verification of Short-Range Order Cluster Model of Six-Component Inconel 718 Alloy Solid Solution. 2.2.2.1. Mass Conservation Analysis. Since the atom conservation has been ensured in the construction process of the above-mentioned solid solution short-range order cluster model for Inconel 718 alloy, only the mass conservation of the cluster model was analyzed here. The atomic content (at%) of each component in the constructed cluster model was converted into the corresponding elemental content (wt%) according to Formula (7) and compared with the elemental content of each component in Inconel 718 alloy selected in this study (as shown in Figure 2). The results showed that the proposed cluster model had high consistency and met the mass conservation criterion.

$$\begin{aligned} A(\text{mass\%}) = {} & \{A(\text{at\%}) \times \text{relative atomic mass of A}]/\{[100 - A(\text{at\%})] \\ & \times \text{relative atomic mass of B}+[A(\text{at\%}) \times \text{relative atomic mass of A}]\}\} \\ & \times 100\%(\text{AB alloy for example}) \end{aligned} \quad (7)$$

2.2.2.2. Atomic Stacking Energy Analysis. In view of the strong interaction between neighboring atoms in both the crystalline structure and the liquid structure of amorphous solid solution, which results in the formation of short-range ordered clusters, the cluster structure or crystal structure will have the closest atomic stack under such strong interatomic interaction when the corresponding cluster structure or phase is formed. Therefore, the principle of minimum energy of Friedel oscillation caused by internal electron interaction caused by atomic stacking proposed in section 2.1.2 above will be met.

In combination with the relationship between the atomic distribution and the Friedel oscillation potential function established in section 2.1.2 (as shown in Figure 4), in the atomic density distribution function, the cluster model was further decomposed into three parts, i.e., central atoms, first shell atoms and externally connected atoms in the first shell, according to the spatial distribution structure of the constructed cluster model. Second, the atomic distribution density $g(r)$ under the specific number of atoms included in the connecting atoms from the central atom to the first shell and from the central atom to the outside of the first shell was sequentially calculated by Formula (3). At the same time, in order to uniformly compare the atomic distribution density function directly with the Friedel oscillation potential function generated by the corresponding electrons, the distance from each shell layer to the center atom was calculated as the weighted average r_1, and then the atomic density radial distribution functions of each shell layer in the solid solution short-range order cluster of Inconel 718 alloy were drawn by normalizing the distance in $g(r)$ (i.e., $\lambda_{Fr} = r_1/1.25$, **the abscissa of the atomic density distribution function** $= r/\lambda_{Fr}$). It was found that the densest stacking position of the first shell of the cluster model was close to 1.25, while the most evacuated stacking position of the corresponding externally connected atoms was close to 1.75 and close to the ideal cluster model structure shown in Figure 4. Therefore, the overall system energy of the solid solution cluster model of Inconel 718 alloy established in this paper is the smallest and the most stable, which can reasonably and accurately quantitatively reflect the atom distribution and mass occupancy of the solid solution of the selected Inconel 718 nickel-base superalloy, and thus the final cluster structure as shown in Figure 6b is obtained.

2.3. A Quantitative Expression of Resistivity Based on Short-Range Order Cluster Model of Alloy Solid Solution. As the above cluster model averages the atomic arrangement structure of the solid solution of Inconel 718 nickel-base superalloy into the first shell and its external connecting atomic structure units, and considering the high solute concentration of Inconel 718 nickel-base superalloy used in this paper, the whole solid solution structure tends to be more orderly in the whole process. On the basis of these two aspects, although the real solid solution may have multilayer disorder in the vicinity of the short-range order cluster, no matter how many layers are mainly concentrated in the core where the cluster atoms are most densely accumulated and in the adjacent shell from the impurity density of scattered electron waves, the connecting atoms outside the shell layer and their out-of-order degree make little contribution to the scattering of resistivity judging from the impurity density of scattered electron waves. In addition, considering that the resistivity inside the alloy is mainly caused by the scattering of

https://doi.org/10.1021/acsomega.2c07644
ACS Omega 2023, 8, 11987−11998

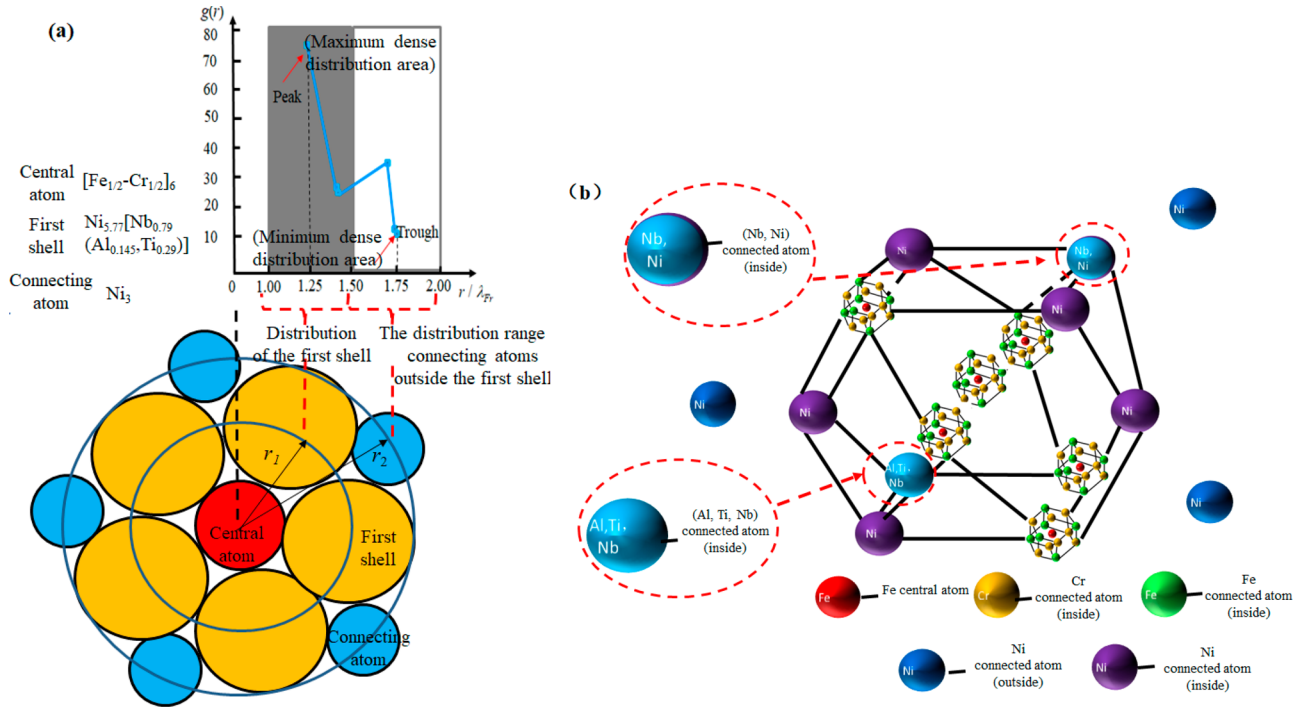

Figure 6. Radial distribution of atomic density in each shell of solid solution cluster model in (a), and the atomic spatial distribution structure of solid solution cluster model of Inconel 718 nickel-base superalloy in (b).

atoms in the crystal structure, and combining with the law of conservation of materials (atomic conservation), the corresponding atomic content of the alloy always keeps the same under different forming states. In addition, the additional electron scattering caused by lattice distortion during precipitation of the precipitated phase is much smaller than the electron scattering effect generated when the matrix is in solid solution with atoms, so that the resistivity of the alloy can be approximately understood as the superposition contribution of the resistivity of various atoms at different contents in the center part of the solid solution cluster model and in the adjacent shell part. Therefore, the idea of distributing resistivity to the close-packed atoms in the central part of the solid solution cluster model and the adjacent shell part is put forward to approximate the resistivity of multicomponent alloys with different element compositions. First, the number of atoms contained in the cluster structure of pure metal was counted to obtain the contribution of various kinds of atoms to resistivity. Second, the total resistivity with specific atomic content (at%) of the corresponding solid solution cluster model with different alloy element content (wt%) was obtained by weighting according to the atomic content distribution in the center of the solid solution cluster model and the adjacent shell part.[51,52]

For the cluster model of Inconel 718 nickel-base superalloy (HSA) established in this paper ($[Fe_{1/2}\text{-}Cr_{1/2}]_6[Nb_{0.79}$ $(Al_{0.15}$, $Ti_{0.29})]$ $Ni_{5.77}\text{-}Ni_3$), the atomic dense stacking area is mainly concentrated in the first shell ($[Nb_{0.79}$ $(Al_{0.15},Ti_{0.29})]$ $Ni_{5.77}$) nearest to the core ($[Fe_{1/2}\text{-}Cr_{1/2}]_6$). Second, by analyzing the cluster structure and resistivity of pure Fe, Cr, Nb, Al and Ti metals, the corresponding resistivity of each atom with 1%at content can be calculated as (25 °C):

$$\rho_{Fe(1at\%)} = 4.87 \times 10^{-5}(\Omega\cdot mm),\ \rho_{Cr(1at\%)} = 7.66 \times 10^{-5}(\Omega\cdot mm)$$
$$,\ \rho_{Nb(1at\%)} = 1.15 \times 10^{-5}(\Omega\cdot mm),\ \rho_{Al(1at\%)} = 0.67 \times 10^{-5}(\Omega\cdot mm)$$
$$,\ \rho_{Ti(1at\%)} = 21.05 \times 10^{-5}(\Omega\cdot mm),\ \rho_{Ni(1at\%)} = 1.72 \times 10^{-5}(\Omega\cdot mm)$$

Meanwhile, considering that the above calculation was performed by converting all atoms in the core cluster into one atom (i.e., $[Fe_{1/2}\text{-}Cr_{1/2}]$) in the construction of this cluster model, and the conductivity should be enlarged to the original proportion in combination with its content in the calculation, the same is true for the shell part. Thus, so that the alloy resistivity of Inconel 718 nickel-base superalloy under HSA heat treatment can be expressed as shown in the following formula $\rho_t = \rho_c + \rho_f = 94.19 + 42.59 = 136.78 \times 10^{-5}\Omega\cdot mm = 1.37 \times 10^{-3}(\Omega\cdot mm)$ Where,ρ_t represents alloy total resistivity; ρ_c represents core cluster resistivity; ρ_f represents nearest neighbor clusters for shell part resistivity.

In order to further highlight the characteristics of this study, the component design of the alloy was also correlated with the alloy solid resistivity. That is, according to the Inconel 718 cluster construction method in sections 2.1 and 2.2 and the relevant conservation formula 6 and formula 7, and by analyzing the content of each element and its contribution to the related alloy resistivity, the design (each element content of Inconel 718 alloy (wt%)) of the Min/Max resistivity of Inconel 718 alloy under the AMS 5383/AMS 5662 standard is calculated (as shown in Table 3). At the same time, the alloy was prepared with each high purity element (99.99 wt %), weighed by FA2004 electronic scale and WK nonself-consuming vacuum arc furnace, and the predicted resistivity under the guidance of the above theoretical model was verified by the solid resistance tester. The accuracy of the proposed method in the alloy resistivity prediction was also well demonstrated based on the results shown in Table 3. Thus,

https://doi.org/10.1021/acsomega.2c07644
ACS Omega 2023, 8, 11987−11998

Table 3. Composition Design of Inconel 718 Alloy at Different Resistivity

Composition of main elements of Inconel 718 alloy (high resistivity) (wt %)			
Element	Content	Element	Content
Al	0.2900	Fe	Remainder
Cr	21.0000	Nb	5.5000
Ti	1.1500	Ni	55.0000
Corresponding cluster model	$[Fe_{0.35}\text{-}Cr_{0.65}]_6[Nb_{0.6}(Al_{0.1}, Ti_{0.22})]$ $Ni_{6.08}\text{-}Ni_3$ ($\rho_t = \rho_c + \rho_f$ = 100.25 + 39.61 = 139.87 × 10^{-5}Ω·mm = 1.40 × 10^{-3}(Ω·mm))	Actual resistivity of the alloy	1.39 × 10^{-3} (Ω·mm)
Composition of main elements of Inconel 718 alloy (high resistivity) (wt %)			
Element	Content	Element	Content
Al	0.8000	Fe	Remainder
Cr	17.0000	Nb	5.5000
Ti	0.7000	Ni	55.0000
Corresponding cluster model	$[Fe_{0.5}\text{-}Cr_{0.5}]_6[Nb_{0.55}(Al_{0.3}, Ti_{0.15})]$ $Ni_6\text{-}Ni_3$ ($\rho_t = \rho_c + \rho_f$ = 94.19 + 35.78 = 129.97 × 10^{-5}Ω·mm= 1.30 × 10^{-3}(Ω·mm))	Actual resistivity of the alloy	1.30 × 10^{-3} (Ω·mm)

the corresponding element design with the highest and lowest resistivity of the alloy is obtained.

2.4. Cluster Model Construction and Corresponding Resistivity Expression of Other Multicomponent Alloys.

In addition, in order to extend the proposed method in multicomponent alloys, this paper also taken Al−Cu alloy as an example, and the casting cluster model and related resistivity of ZL205A alloy were predicted.

Based on the above cluster model construction method in section 2.1 to 2.3, and the phase of casting ZL205A alloy was mainly composed of Al_2Cu and Al (according to XRD analysis of ZL205A casting), the specific cluster formation process will not be described too much, and the related cluster model formation process was shown in Figure 7.

According to Figure 7 for ZL205A alloy cluster construction, the corresponding cluster model constructed in this study was: $[Al_9-Cu_4]$-Al_1Cu_1, and this structure can be expressed as the center and first nearest neighbor space structure of Al_9 and Cu_4, with one Al, Cu atom connected externally. Considering that the resistivity of Al and Cu were: $\rho_{Al(1\ atom\ \%)}$ = 0.68 × 10^{-5}(Ω·mm), $\rho_{Cu(1\ atom\ \%)}$ = 0.43 × 10^{-5}(Ω·mm), respectively, the ZL205A alloy conductivity under this structure is calculated to be 7.84 × 10^{-5}(Ω·mm)(25 °C). The resistivity measurements and comparison of actual cast ZL205A alloys 7.98 × 10^{-5}(Ω·mm)25 °C) also verified that the method proposed here in this study has a high prediction level in other carbide alloys.

Besides, to verify and popularize the rationality and accuracy of this method, based on the calculation of resistivity of Inconel 718 nickel-base superalloy by this method, the resistivity of multiphase alloys such as two-component Ni−Ti memory alloy, three-component 1J series soft magnetic alloy, three-component Cu−Ni−Mo superconducting alloy, four-component Cr-Ni-Fe-Si electrothermal alloy and those for other non-nickel alloys were also predicted respectively (as shown in Table 4). The error between the predicted value and the actual measured value (by using the KDB-I type four-probe resistivity tester manufactured by Guangdong Kunde Technology Co., Ltd.) was basically controlled within the range of 5%, showing a high characterization accuracy.

3. RESULTS AND DISCUSSION

Although simple metals are often used in engineering practice to improve the physical properties of metals by alloying, the lack of awareness about the origin of the formation of industrial alloys results in the components of high-quality alloys being derived from a large amount of empirical exploration over a long period of time, and a large amount of energy and financial resources are wasted on the research and development of new alloys. Considering that the solid solutions of multicomponent alloys are ordered in short-range, it is necessary to deeply study and establish the microatomic structure root behind the alloy components and correlate with the corresponding macro-physical properties, so as to guide the development of high-performance multicomponent alloys through effective composition theory design. In this study, Inconel 718 multicomponent alloy, which has been developed and applied widely and frequently in recent years, was taken as a research object. Based on the qualitative method of "nearest neighbor cluster + connecting atoms" proposed by predecessors to characterize the short-range atom arrangement structure of multicomponent alloy solid solution, the quantitative accurate expression aiming at the micro short-

https://doi.org/10.1021/acsomega.2c07644
ACS Omega 2023, 8, 11987−11998

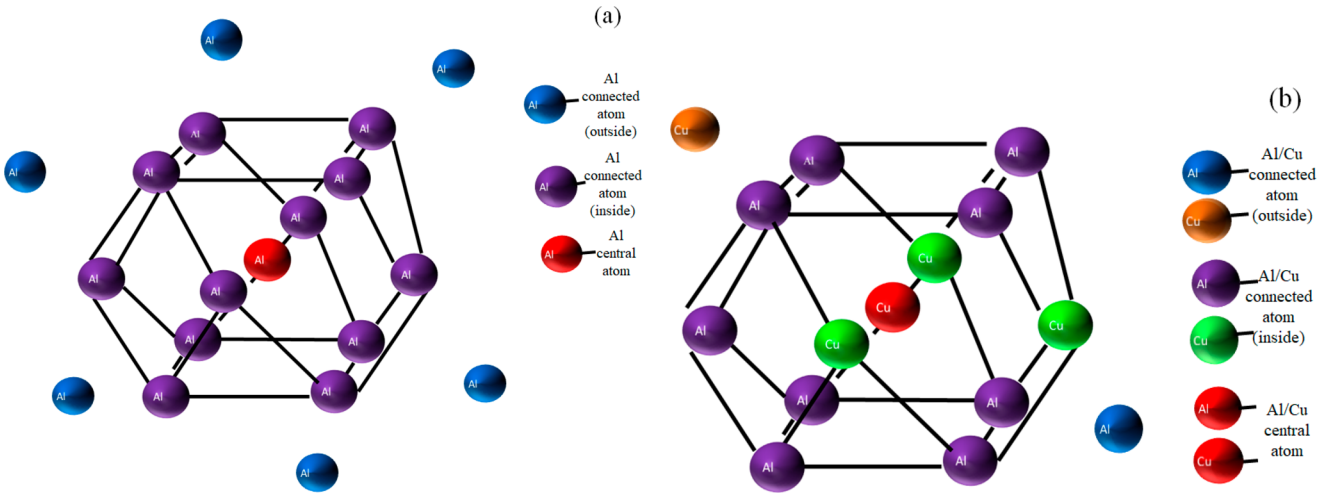

Figure 7. Short-range order cluster model of pure Al matrix in (a), and short-range order cluster model of ZL205A solid solution in (b).

Table 4. Prediction Results of Resistivity of Various Multiphase Alloy Materials (20°C)

Types of alloy	Solid solution cluster model	Predicted resistivity 10^{-3} (Ω·mm)	Actual resistivity 10^{-3} (Ω·mm)	Error (%)
SLM molded Inconel 718 nickel-base superalloy	$[Fe_{1/2}\text{-}Cr_{1/2}]_6[Nb_{0.79}(Al_{0.15},Ti_{0.29})]$ $Ni_{5.77}\text{-}Ni_3$	1.37 (25 °C)	1.32 (25 °C)	5.0
Red copper	Cu_{13}	0.017 (25 °C)	0.0165 (25 °C)	3.0
Ni-Ti memory alloy	$Ni_{5.90}Ti_{7.10}$	0.598	0.570	4.9
1J46 Fe-Ni soft magnetic alloy with high permeability and high saturation magnetic induction strength	$Fe_{7.20}Ni_{5.80}$	0.448	0.450	0.5
1J34 Fe-Ni-Co Rectangular magnetic alloy	$[Co_{0.44}Fe_{0.56}]_{8.58}\text{-}Ni_{4.42}$	0.483	0.500	3.4
1J86 Ni-Fe-Mo soft magnetic alloy with high initial permeability	$[Mo_{0.25}Fe_{0.75}]_{2.15}\text{-}Ni_{10.85}$	0.568	0.600	5.3
Cu-Ni-Mo superconducting alloy (different component ratios)	$[Mo_{1/13}Ni_{12/13}]_{3.00}\text{-}Cu_{10.00}$	0.054	0.052	3.8
	$[Mo_{4/13}Ni_{9/13}]_{3.00}\text{-}Cu_{10.00}$	0.043	0.042	2.4
	$[Mo_{6/13}Ni_{7/13}]_{3.00}\text{-}Cu_{10.00}$	0.039	0.040	2.5
	$[Mo_{2/14}Ni_{12/14}]_{5.00}\text{-}Cu_{8.00}$	0.083	0.081	2.5
	$[Mo_{4/16}Ni_{12/16}]_{5.00}\text{-}Cu_{8.00}$	0.072	0.071	1.4
	$[Mo_{6/18}Ni_{12/18}]_{5.00}\text{-}Cu_{8.00}$	0.064	0.065	1.5
Cr20-Ni35-Fe45-Si Electrothermal alloy	$[Cr_{0.33}Fe_{0.67}]_{8.75}Si_{0.03}\text{-}Ni_{4.22}$	1.038	1.000	3.8
Cu-Zn C28000 alloy	$[Zn\text{-}Cu_{12}]Zn_{7.58}$	0.032	0.033	3.1
Al-Cu C60600 alloy	$[Al\text{-}Cu_{12}]Al_1Cu_4$	0.033	0.032	3.0
Cu-Be C17200 alloy	$[Cu\text{-}Cu_{12}]Be_2Cu_2$	0.009	0.100	1.0
ZL205A cannon steel alloy	$[Al_9\text{-}Cu_4]\text{-}Al_1Cu_1$	0.078	0.080	2.6

range order cluster spatial structure of the multicomponent alloy solid solution was innovatively provided, and the accurate guidance on the conductive performance of multicomponent system high-temperature alloy and high-entropy alloy materials under the construction of the short-range order cluster model was realized through the contribution influence of the spatial distribution content of each atom in the multicomponent alloy on the external current electron scattering rate, and the specific work is summarized as follows: 1) According to the formation mechanism of Inconel 718 multicomponent alloy, a three-component Ni−Cr−Fe solid solution short-range order cluster model with a large number of solid solution elements added was qualitatively constructed in combination with the solid solution solubility and atomic mixing enthalpy criterion. At the same time, the short-range order cluster model of three-component Ni−Cr−Fe solid solution was quantitatively expressed by introducing the Friedel oscillation potential function generated due to interaction between electrons in solid solution atoms and being correlated with the radial density of corresponding atomic arrangement; 2) Based on the three-component system solid solution model, a six-component system Inconel 718 alloy solid solution short-range order cluster model added with trace strengthening elements was qualitatively constructed by further combining the solid solution solubility and the atomic mixing enthalpy criterion. Then, the method for constructing the nearest neighbor cluster in the alloy phase, which is defined by the maximum density of atoms radially arranged so as to meet the minimum principle of energy stacking, was provided, the corresponding atomic content of an Inconel 718 alloy solid solution short-range order cluster model formed by adding trace elements was determined, and the accuracy and rationality of the construction of the multicomponent alloy cluster model were determined by combining element mass conservation, atom conservation and atom space stacking atoms; 3) According to the influence of the spatial distribution content of each atom in the multicomponent alloy on the external current electron scattering rate (i.e., resistivity), and through the thought of weighting the resistivity by the atomic content of each component, the accurate analysis of the conductive performance of the multicomponent alloy was finally realized (the prediction rate is within 5%) by using the alloy solid solution

https://doi.org/10.1021/acsomega.2c07644
ACS Omega 2023, 8, 11987−11998

short-range order cluster model. Finally, the accurate guidance on the conductive performance of the multicomponent system high-temperature alloy and the high-entropy alloy material under the construction of the short-range order cluster model was realized, laying a theoretical basis and research guarantee for subsequent design and research and development of superalloy components with high physical properties.

However, in order to improve the computational efficiency, the electrical resistivity interaction of different elements in solid solution was ignored when constructing the resistivity model guided by the above multiphase alloy clusters. Therefore, when the resistivity under the guidance of cluster model is constructed in the future, further consideration of this problem will improve the accuracy performance and prediction ability of the model more accurately.

AUTHOR INFORMATION

Corresponding Author

Liang Huang − *Mechatronic Engineering, Xi'an Technological University, Xi'an 710048, China;* orcid.org/0000-0002-9968-139X; Phone: 029-86173054; Email: huangliang@xatu.edu.cn

Authors

Yan Cao − *Computer Science and Engineering, Xi'an Technological University, Xi'an 710048, China;* orcid.org/0000-0002-2959-5533

Shoumin Wang − *Mechatronic Engineering, Xi'an Technological University, Xi'an 710048, China*

Gaohong Li − *Materials and Chemical Engineering, Xi'an Technological University, Xi'an 710021, China*

Hao Dong − *Computer Science and Engineering, Xi'an Technological University, Xi'an 710048, China*

Tao Wu − *Graduate School, Xi'an Technological University, Xi'an 710021, China*

Ning Wang − *Advanced Manufacturing Research Institute, Xi'an KunLun Industry (Group) Company with Limited Liability, Xi'an 710043, China*

Complete contact information is available at: https://pubs.acs.org/10.1021/acsomega.2c07644

Author Contributions

Conceptualization, L.H. and Y.C.; methodology, L.H. and S.W.; validation, L.H., G.L., and H.D.; formal analysis, L.H. and T.W.; investigation, N.W. and T.W.; resources, L.H.; writing−original draft preparation, L.H. and Y.C.; writing−review and editing, L.H.; project administration, Y.C. and S.W.; funding acquisition, Y.C. and L.H.

Funding

This research is funded by National Natural Science Foundation of China (NSFC) under grant number 52275508, the project of 2019 Yulin Science and Technology Program under grant number K20190176, and the Xi'an Science and Technology Bureau, universities and institutes of science and technology personnel service enterprise project under grant number 22GXFW0051, and the Natural Science Basic Research Program of Shaanxi Province under grant number 2023-JC-QN-0392.

Notes

The authors declare no competing financial interest.

REFERENCES

(1) Wang, T.-L.; Khan, M. A.; Feng, C.-S.; Lin, M.-Z.; Yasin, G.; Liao, W.-B. Parallel preparation of multi-component alloys with composition gradient distribution and their nonlinear microstructures and mechanical properties. *J. Alloys Compd.* **2022**, *921*, 166159.

(2) Qiao, L.; Lai, Z.; Liu, Y.; Bao, A.; Zhu, J. Modelling and prediction of hardness in multi-component alloys: A combined machine learning, first principles and experimental study. *J. Alloys Compd.* **2021**, *853*, 156959.

(3) Cao, S. C.; Lu, W. Q.; Hu, Q. D.; Yu, P. F.; Ge, X.; Lai, P. S.; Li, J. G. Atomic tuning effect of TiB2 particles on the liquid phase separation behavior of an Al-Bi immiscible alloy. *Scripta Materialia* **2022**, *209*, 114365.

(4) Zhifang, W.; Chao, L.; Run, W.; Qingming, C. Coarsening kinetics of Pb phase in a nanocomposite alloy produced by mechanical alloying in immiscible Al-Pb system and the influence of Cu addition on it. *Rare Metal Materials and Engineering* **2017**, *46* (12), 3675−3681.

(5) Liu, Z. H.; Wang, Q. Z.; Guo, S. N.; Zhang, X.; Wang, Y. K.; Jiang, T. L.; Wang, H. L.; Zhang, S.; Jiang, W. W.; Liu, S. M.; et al. The preliminary exploration of composition origin of solid solution alloys used in thermocouple by cluster-plus-glue-atom model. *Materials & Design,* **2022**, *216*, 1−9.

(6) Valiev, R.Z.; Murashkin, M. Y.; Sabirov, I. A nanostructural design to produce high-strength Al alloys with enhanced electrical conductivity. *Scripta Materialia* **2014**, *76*, 13−16.

(7) Guan, K.; Egami, M.; Egusa, D.; Kimizuka, H.; Yamasaki, M.; Kawamura, Y.; Abe, E. Short-range order clusters in the long-period stacking/order phases with an intrinsic-I type stacking fault in Mg-Co-Y alloys. *Scripta Materialia* **2022**, *207*, 114282.

(8) Bragg, W. L.; West, J. X. A technique for the X-ray examination of crystal structures with many parameters. *Crystalline Materials* **1929**, *69*, 1−6.

(9) Bernal, J. D. A geometrical approach to the structure of liquids. *Nature* **1960**, *185*, 68−70.

(10) Chen, J.-X.; Qiang, J.-B.; Wang, Q.; Don, C. Defining nearest neighbor clusters in alloy phases using radial distribution of atomic density. *Acta Physics Sinca* **2012**, *61* (4), 046102.

(11) Mackay, A.; Finney, J.; Gotoh, K. The closest packing of equal spheres on a spherical surface. *Acta Crystallogr., Sect. A* **1977**, *33* (1), 98−100.

(12) Zhang, S.; Liu, T. Y.; Zou, C. L.; Zhao, Y. J.; Hu, X. G.; Dong, C. Composition interpretation of Co-Cr industrial alloys using cluster formula approach. *Materials Today Communications* **2023**, *34*, 104922.

(13) Yang, M.; Hu, Y. L.; Li, X. N.; Li, Z. M.; Zheng, Y. H.; Li, N. J.; Dong, C. Compositional interpretation of high elasticity Cu−Ni−Sn alloys using cluster-plus-glue-atom model. *Journal of Materials Research and Technology* **2022**, *17*, 1246−1258.

(14) Zhu, Z. H.; Liu, T. Y.; Dong, C.; Dong, D. D.; Zhang, S.; Wang, Q. Achieving high-temperature strength and plasticity in near-α Ti-7Al-3Zr-2V alloy using cluster formula design. *Journal of Materials Research and Technology* **2022**, *18*, 2582−2592.

(15) Liu, T. Y.; Min, X. H.; Zhang, S.; Wang, C. S.; Dong, C. Microstructures and mechanical properties of Ti−Al−V−Nb alloys with cluster formula manufactured by laser additive manufacturing. *Transactions of Nonferrous Metals Society of China* **2021**, *31* (10), 3012−3023.

(16) Miracle, D. B. The efficient cluster packing model-an atomic structure model for metallic glasses. *Acta Materila* **2006**, *54* (16), 4317−4336.

(17) Ma, R. T.; Hao, C. P.; Wang, Q.; Ren, M.; Wang, Y.; Dong, C. Cluster-plus-glue-atom model and composition design of BCC Ti-Mo-Nb-Zr solid solution alloys with low young's modulus. *Acta Metal Sinica* **2010**, *46* (9), 1034−1040.

(18) Liu, P; Tian, B. H.; Zhao, D. M. *Copper alloy functional material.* Science press, Beijing, 2004: 76−82.

(19) Zhu, S. Y.; Yang, Q. K.; Gan, K. F.; Yan, D. S.; Zhang, Y.; Liu, C.; Li, Z. M. A strong ferritic high-resistivity multicomponent alloy

with tunable ordered coherent multicomponent nanoprecipitates. *Acta Mater.* **2022**, *238*, 118209.
(20) You, D.; Zhang, H.; Ganorkar, S.; Kim, T.; Schroers, J.; Vlassak, J. J.; Lee, D. Electrical resistivity as a descriptor for classification of amorphous versus crystalline phases of alloys. *Acta Mater.* **2022**, *231*, 117861.
(21) Bao, S.; Guo, X. W.; Wang, Z. L.; Zhao, Q.; Liu, Y. L.; Meng, F. S.; Sun, B. Z.; Jia, N.; Qi, Y. Short range ordering improves elastic properties of Mo additive W-Re solid solution: A first principles investigation. *Scripta Materialia* **2023**, *224*, 115132.
(22) Abu-Odeh, A.; Asta, M. Modeling the effect of short-range order on cross-slip in an FCC solid solution. *Acta Mater.* **2022**, *226*, 117615.
(23) Cowley, J. X-Ray measurement of order in in Cu3Au. *J. Appl. Phys.* **1950**, *21* (1), 24−30.
(24) Liu, H. G.; Tang, S.; Ma, Y. Z.; Liu, W. S.; Liang, C. P. Short-range ordering governs brittleness and ductility in W-Ta solid solution: Insights from Pugh's shear-to-bulk modulus ratio. *Scripta Materialia* **2021**, *204*, 114136.
(25) He, Q.F.; Tang, P.H.; Chen, H.A.; Lan, S.; Wang, J.G.; Luan, J.H.; Du, M.; Liu, Y.; Liu, C.T.; Pao, C.W.; Yang, Y. Understanding chemical short-range ordering/demixing coupled with lattice distortion in solid solution high entropy alloys. *Acta Materialia,* **2021**, *216*, 117140.
(26) Bradley, A; Jay, A. The formation of superlattices in alloys of iron and aluminium. *Proceedings of the Royal Society of London, Series A, Contating Papers of a Mathematical and Physical Character*, The Royal Society, UK, 1932, *136* (829), 210−232.
(27) Tian, S; Li, X. C.; Li, B. S. *Physical properties of metals*. National defence of Industry Press, Beijing, 1985: 24−34.
(28) Tanimoto, H.; Hozumi, R.; Kawamura, M. Electrical resistivity and short-range order in rapid-quenched CrMnFeCoNi high-entropy alloy. *J. Alloys Compd.* **2022**, *896*, 163059.
(29) Gu, T. Relationship between the short-range order and electrical resistivity in liquid indium-antimony. *J. Non-Cryst. Solids* **2012**, *358* (16), 1892−1896.
(30) Borgiel, W.; Stysiak, D.; Gonsior, M.; Lipowczan, M. Influence of the short range order (SRO) on electrical resistivity of the magnetic rare earth metals in the paramagnetic region. *J. Alloys Compd.* **2007**, *442* (1), 139−141.
(31) Mouas, M.; Fazel, N.; Gasser, F.; Golovin, I. S.; Gasser, J. G. Kinetics of the L12 ↔ D019 transition for Fe3Ga-type alloy determined by in situ electrical resistivity. *Mater. Lett.* **2023**, *334*, 133731.
(32) Liu, K. M.; Lu, D. P.; Zhou, H. T.; Atrens, A.; Zou, J.; Yang, Y. L.; Zeng, S. M. Effect of Ag micro-alloying on the microstructure and properites of Cu-14Fe in situ composite. *Materials Science and Engineering A-Structural Materials Properties Microstructure and Processing* **2010**, *527*, 4953−4958.
(33) Dong, C; Wang, Q; Qiang, J B; Wang, Y M; Jiang, N; Han, G; Li, Y H; Wu, J; Xia, J H Effect of magnesium on microstructure and properties of Cu-Cr alloy. *J. Phys. D: Appl. Phys.* **2007**, *40* (15), R273−R291.
(34) Mackay, A. L.; Finney, J. L.; Gotoh, K. The closest packing of equal spheres on a spherical surface. *Acta Crystallographica Section A: Crystal Physics, Diffraction, Theoretical and General Crystallography* **1977**, *33* (1), 98−100.
(35) Mackay, A. L.; Finney, J. L. Structuration. *J. Appl. Crystallogr.* **1973**, *6* (4), 284−289.
(36) Hosseini, E.; Popovich, V.A. A review of mechanical properties of additively manufactured Inconel 718. *Additive Manufacturing* **2019**, *30*, 100877.
(37) Chen, C. J.; Zhang, M.; Zhang, S. C.; Chang, Q. M.; Chen, X. Study on NiCrAl coating alloyed on In 718 Ni-base alloy by high-energy micro-arc alloying processing. *Advanced Science Letters* **2011**, *4* (3), 996−1001.
(38) Murakami, M.; Nomura, N.; Doi, H.; Tsutsumi, Y.; Nakamura, H.; Chiba, A.; Hanawa, T. Microstructures of Zr-added Co-Cr-Mo alloy compacts fabricated with a metal injection molding process and their metal release in 1mass% lactic acid. *Materials Transactions* **2010**, *51* (7), 1281−1287.
(39) Tang, X.; Thompson, G. B.; Ma, K.; Weinberger, C. R. The role of entropy and enthalpy in high entropy carbides. *Comput. Mater. Sci.* **2022**, *210*, 111474.
(40) Friedel, J. Metallic alloys. *Il Nuovo Cimento* **1958**, *7*, 287−311.
(41) Bena, C. Friedel oscillations: Decoding the hidden physicsLes oscillations de Friedel: decoder la physique cachée. *Comptes Rendus Physique* **2016**, *17* (3), 302−321.
(42) Villain, J.; Lavagna, M.; Bruno, P. Jacques Friedel and the physics of metals and alloys. *Comptes Rendus Physique* **2016**, *17* (3), 276−290.
(43) Johann, K. Evidence of icosahedral short-range order in Zr70Cu30 and Zr70Cu29Pd1 metallic glasses. *Appl. Phys. Lett.* **2003**, *83* (10), 3924−3926.
(44) Duan, G.; Xu, D.; Zhang, Q.; Zhang, G.; Cagin, T.; Johnson, W. L.; Goddard, W. A. Erratum: molecular dynamics study of the binary Cu46Zr54 metallic glass motivated by experiments: glass formation and atomic-level structure. *Phys. Rev. B* **2006**, *74* (1), 019901.
(45) Galvan-Colin, J.; Valladares, A. A.; Valladares, R. M.; Valladares, A. Short-range order in ab initio computer generated amorphous and liquid Cu−Zr alloys: A new approach. *Physica B: Condensed Matter* **2015**, *475*, 140−147.
(46) Zhang, L.; Wu, Y.; Bian, X.; Li, H.; Wang, W.; Wu, S. Short-range and medium-range order in liquid and amorphous $Al_{90}Fe_5Ce_5$ alloys. *J. Non-Cryst. Solids* **2000**, *262* (3), 169−176.
(47) Luo, L. J.; Chen, H.; Wang, Y. M.; Qiang, J. B.; Wang, Q.; Dong, C.; Haeussler, P. 24 Electron cluster formulas as the 'molecular' units of ideal metallic glasses. *Philos. Mag.* **2014**, *94* (22), 2520−2540.
(48) Wu, Z. W.; Li, M. Z.; Wang, W. H.; Liu, K. X. Hidden topological order and its correlation with glass-forming ability in metallic glasses. *Nat. Commun.* **2015**, *6*, 6035.
(49) Ding, J.; Cheng, Y.; Ma, E. Charge-transfer-enhanced prism-type local order in amorphous $Mg6_5Cu_{25}Y_{10}$: Short-to-medium-range structural evolution underlying liquid fragility and heat capacity. *Acta Mater.* **2013**, *61* (8), 3130−3140.
(50) Mauro, N. A.; Bendert, J. C.; Vogt, A. J.; Gewin, J. M.; Kelton, K. F. High energy X-ray scattering studies of the local order in liquid Al. *J. Chem. Phys.* **2011**, *135* (4), 044502.
(51) Parkin, C.; Moorehead, M.; Elbakhshwan, M.; Hu, J.; Chen, W.-Y.; Li, M.; He, L.; Sridharan, K.; Couet, A. In situ microstructural evolution in face-centered and body-centered cubic complex concentrated solid-solution alloys under Heavy Ion Irradiation. *Acta Mater.* **2020**, *198*, 85−99.
(52) Ferasat, K.; Osetsky, Y. N.; Barashev, A. V.; Zhang, Y.; Yao, Z.; Beland, L. K. Accelerated kinetic monte carlo: A case study; vacancy and dumbbell interstitial diffusion traps in concentrated solid solution alloys. *J. Chem. Phys.* **2020**, *153* (7), 074109.

https://doi.org/10.1021/acsomega.2c07644
ACS Omega 2023, 8, 11987−11998